Chapter 1

Current Applications of Optical Coherence Tomography in Ophthalmology

Nadia Al Kharousi, Upender K. Wali and Sitara Azeem

Additional information is available at the end of the chapter

http://dx.doi.org/10.5772/53961

1. Introduction

Optical coherence tomography (OCT) was first reported in 1991 as a non-invasive, cross-sectional ocular imaging technology (Huang et al., 1991) and today is the most promising non-contact, high resolution tomographic and biomicroscopic imaging device in ophthalmology. It is a computerized instrument structured on the principle of low-coherence interferometry (Huang et al., 1991; Hrynchak & Simpson., 2007) generating a pseudo-color representation of the tissue structures, based on the intensity of light returning from the scanned tissue. This noninvasive, noncontact and quick imaging technique has revolutionized modern ophthalmology practice. The current applications of OCT have been improvised and expanded dramatically in precision and specificity in clinical medicine and industrial applications. In medicine, the technique has been compared to an in-vivo optical biopsy. As the resolution of OCT has been improving with time, the localization and quantification of the tissues has accordingly, become more refined, faster and predictable (Ryan SJ, 2006). What was initially and mainly a posterior segment procedure, OCT has now wider applications in anterior segment of the eye as well. The first anterior segment OCT (AS-OCT) was available in 1994. Its current use in cornea and refractive surgery including phakic intraocular lens implantation, laser-assisted in situ keratomileusis (LASIK) enhancement, lamellar keratoplasty and intraoperative OCT has opened promising therapeutic and diagnostic options in both research and clinical applications in ophthalmology. With an improved scan speed and resolution, the new models of spectral-domain (SD)-OCT allow measurements with an even lower variability (Leung et al., 2009). Due to reduced measurement errors, e.g. due to motion artifacts, the precision to track and interpret tissues has increased sharply (Leung et al., 2011). OCT is intended for use as a diagnostic device to aid in the detection and management of ocular diseases, however, it is not intended to be used as the sole aid for the diagnosis. Ultra-high

resolution (UHR) OCT is a new imaging system that is being used in several clinical and research purposes. It is an objective technique and has been used for evaluation of tear fluid dynamics, contact lens fitting, imaging of corneal structures, and to describe the characteristics of epithelium, stroma and Descemet's membrane in corneal dystrophies and degenerations (Wang et al., 2010; Shen et al., 2010; Shousha et al., 2010]

2. The machine

There are different models of OCT machine available in the market. This chapter is based on observations made with Cirrus-high definition (HD) spectral domain (SD) OCT (Carl Zeiss Meditech Inc., Dublin, CA; software version 4.0). The light source of OCT is a broadband superluminescent diode laser with a central wavelength of 840 nm. This light generates back-reflections from different intraretinal depths represented by different wavelengths. The acquisition rate of Cirrus-HD-OCT is 27 000 A-scans /second. The axial and transverse resolutions are 15 and 5 μm, respectively. The vast increase in scan speed makes it possible to acquire three-dimensional data sets. Current OCT models are mainly designed for analysis of optic nerve head (optic disc cube), macula and anterior segment of the eye. The tomograms are stored on the computer and/or archive medium, and can be quantitatively analyzed. A CCD video monitors the external eye and assists with scan alignment, while a line scanning ophthalmoscope provides a clear image of the tissue addressed by the scan.

The main hardware components of the OCT include the scan acquisition optics, the interferometer, the spectrometer, the system computer and video monitor. Before scanning the patient looks into the imaging aperture and sees a green star-shaped target against a black background (Figure 1). When scanning stars, the background changes to a bright flickering red, and the patient may see thin bright lines of light, which is the scan beam moving across the field of view. Normally, the patient can look inside the imaging aperture for several minutes at a time without discomfort or tiredness. Patient should be instructed to look at the center of the green target, and not at the moving lights of the scan beam. (Figure 1).

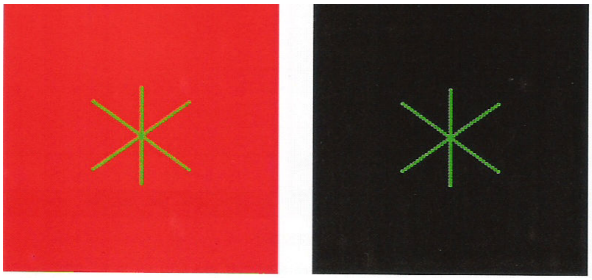

Figure 1. Pattern of targets seen by the patient during OCT procedure.

http://dx.doi.org/10.5772/53961

Anterior segment OCT uses light source with longer infrared wavelengths (1310 nm) to improve the penetration through light scattering tissues, such as sclera and limbus. Unlike posterior segment OCT, AS-OCT requires greater depth of field. AS-OCT also requires higher energy levels than retinal OCT systems. Visualization of retroiridial structures is limited in current AS-OCT, especially in presence of ocular surface opacities and heavy iris pigmentation (Goldsmith et al., 2005]. Currently Cirrus HD-OCT versions 4.0 and 5.0 cannot be used for anterior segment structures, however, one of the latest software updates of Stratus OCT (version 6.0) can measure corneal thickness and visualize structures of the anterior chamber angle.

UHR-OCT uses broadband light sources and has an axial resolution below 5 microns in the tissue.

Intraoperative 3D SD-OCT is the current hot spot in ophthalmology. These systems are separate from the operating microscope and surgery has to be halted while performing the scans. An ideal intraoperative OCT system must be integrated into the operating microscope with a head-up display so that real-time imaging of the operative field can be made without disrupting the surgery (Tang et al., 2010).

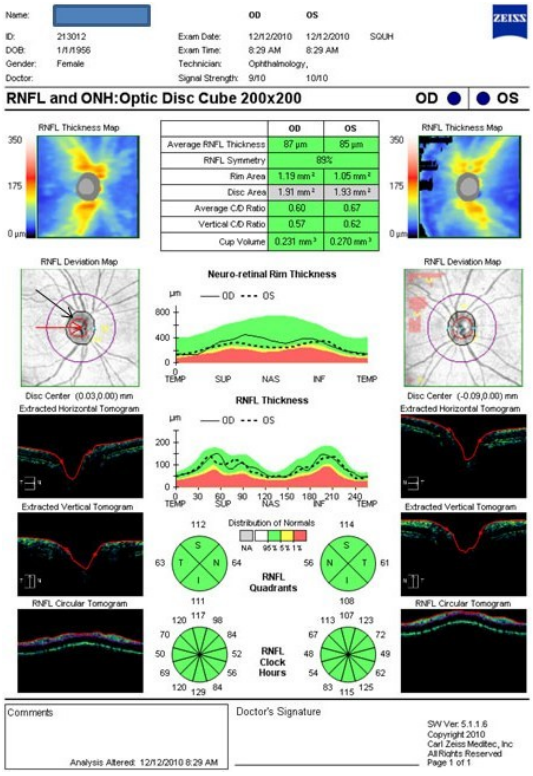

Figure 2. Optic disc cube in a normal patient. See text for details.

2.1. The optic disc cube (Figure 2)

This scan measures the retinal nerve fiber layer (RNFL) thickness in a 6 x 6-mm^2 area consisting of 200 x200 pixels (axial scans). The RNFL thickness is measured at each pixel and a RNFL thickness map is generated. The optic disc (black arrow) and the cup (red arrow) are represented in the center of the scan. A calculation circle of 3.46-mm diameter consisting of 256-A scans is automatically positioned around the optic disc. It is ideal to have signal strength ≥ 6 for the scans. The scan gives an hour-pattern, quadrant-pattern and mean RNFL thickness, which are color coded (white-thickest; green-normal; yellow-borderline, and red-abnormally thin). The printout gives all credible measurements about the RNFL thickness, rim area, disc area, cup-disc ratio and RNFL symmetry.

The scans of two eyes can be compared for symmetry. Latest models can detect saccadic eye movements with the line-scanning ophthalmoscope overlaid with OCT en face during the scanning. Images with motion artifact are rescanned. The SD-OCT has given a precise correlation between optic disc neuroanatomy and histomorphometric reconstruction, which in turn helps understand the pathogenesis in glaucoma (Alexandre et al., 2012; Strouthidis et al., 2009).

2.2. The macular cube (Figure 3)

Generates a cube of data through a 6mm square grid by acquiring a series of 28 horizontal scan lines each composed of 512 A-scans, except for the central vertical and horizontal scans, which are composed of 1024 A-scans each. There are two versions of the macular cube, 512x128 (Figure 3) and 200x200.

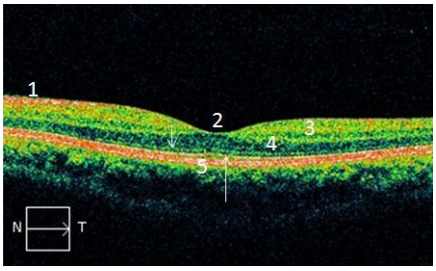

Figure 3. Macular Cube 512x128 in a normal patient. N-Nasal (left hand side of image); T-temporal (right hand side of image). 1-RNFL; 2- Normal foveal depression; 3- plexiform layer (orange-green); 4-Nuclear layer (black); 5-Retinal pigment epithelium (red band of high reflectivity); Short white arrow- External limiting membrane; long white arrow-junction of inner and outer segments of photoreceptors (area of high reflectivity)

The 512 x 128 module has greater resolution in each line from left to right but less resolution from top to bottom. The 200x200 module also has 6mm square grid and acquires 200 horizontal scans each composed of 200 A- scans, except for the central vertical and horizontal scans, which are composed of 1000 A-scans each. Detailed description of the basics of OCT and its images are available on line (Wali & Kharousi., 2012) A 3-D option offers an added advantage in defining the lesions (Figure 4).

http://dx.doi.org/10.5772/53961

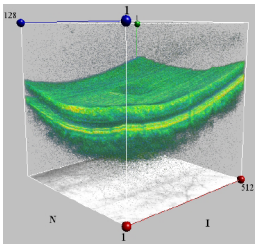

Figure 4. A look-alike of a 3-dimensional figure (here on a 2 dimension surface)

2.3. Anterior segment OCT

This is a custom-built, high speed ultra high resolution device which uses a 3-module superluminescent diode light source allowing an axial resolution of 2 to 3μm. This enables morphologic visualization of conjunctival and corneal architecture. (Shousa et al., 2011 & 2010). The noninvasive nature and quick acquisition time (seconds) makes AS-OCT an ideal imaging technique in handicapped and elderly patients.

3. Current applications of OCT in clinical ophthalmology

Optical coherence tomography provides both qualitative and quantitative (thickness and volume) analyses of the tissues examined in-situ. OCT has been exploited in evaluating both anterior and posterior segments of the eye.

The highest impact of OCT has been in aiding the diagnosis and following the response to treatment and in patients suffering from diabetic retinopathy (DR) (Cruz-Villegas et al., 2004), age-related macular degeneration (ARMD) (Mavro frides et al., 2004) and venous occlusions.

Other applications include imaging morphology and lesions of posterior hyaloid like vitreomacular traction (Figure 5), vitreomacular adhesion (Figure 6) (Kang et al., 2004), detection of fluid within and under the retina which may not be visible clinically. The retinal edema can be measured and localized to different retinal layers. Macular holes (Mavrofrides et al., 2005) and pseudoholes can be more accurately graded, defined and differentiated. Other indications include diagnosis and defining of epiretinal membranes (ERMs) (Mori et al., 2004), retinoschisis (Eriksson et al., 2004), retinal detachment, drug toxicities, RNFL thickness and optic disc parameters.

OCT should not be the only criteria for diagnosis of any ocular disease. Valid perspectives of patient's systemic and ocular disease, clinical examination, fluorescein angiography (FA), indocyanine green angiography (ICGA), biomicroscopy, and above all, the relevant history of the disease process should always be made partner with OCT imaging.

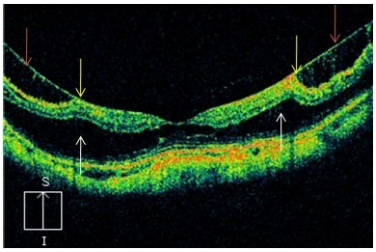

Figure 5. Vitreomacular traction (yellow arrows) by posterior hyaloid membrane (red arrows) causing retinoschisis (white arrows). S-superior (right side of image); I-Inferior (left side of image).

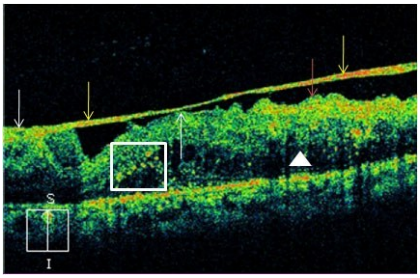

Figure 6. Vitreomacular adhesion: A taught thick posteior hyaloid face (yellow arrows) makes areas of adhesions (white arrow) with the retinal surface producing marked irregularity (bumps) of the retinal tissue (red arrow). Note the hard exudates (white box) and marked retinal thickening due to subretinal fluid (white triangle)

3.1. Anterior segment

There are several advantages of AS-OCT over conventional imaging methods like slit illumination, slit-scanning tomography, Scheimpflug imaging and ultrasound biomicroscopy (UBM). The imaging resolution of AS-OCT is higher than these modalities and gives high resolution cross-sectional 3D images of the anterior segment (Dawczynski et al., 2007; Tan et al., 2011; Goldsmith et al., 2005) Recent models of AS-OCT provide topographic analysis, anterior and posterior elevation maps of the cornea and reliable pachymetric maps (Milla et al., 2011; Nakagawa et al., 2011). It is an ideal research tool to demonstrate ciliary body contraction and lens movement during accommodation (Baikoff et al., 2004).

3.1.1. Cornea and refractive surgery

AS-OCT can be used to determine presurgical parameters in planning different anterior segment procedures. These parameters include anterior chamber depth, crystalline lens rise (distance between anterior pole of crystalline lens and the line joining two iridocorneal angle lines) and anterior chamber angle morphology with reference to the scleral spur (Dawczynski et al., 2007; Tan et al., 2011; Goldsmith et al., 2005). Such parameters can also be used to analyze postsurgical chamber angle dynamics and in intraocular lens (IOL) power calculations (Dinc et al.,

2010; Tan et al., 2011) Phakic IOL is becoming a very popular refractive surgery technique for treatment of high refractive errors. AS-OCT simulates the position of the phakic IOL before surgery by evaluation of anterior segment structures (Mamalis N., 2010). Postoperatively AS-OCT can visualize the contact between the collamer refractive lens and the crystalline lens (Lindland et al., 2010). In cataract surgery AS-OCT has been instrumental in analyzing the structure, integrity and configuration of corneal incisions after cataract surgery (Jagow Von & Kohnen., 2009) yielding information about corneal wound architecture, Descemet's detachment and wound leaks. Studies with AS-OCT have also revealed that corneal epithelial closure after cataract surgery was completed in 1-8 days (Can et al., 2011; Torres et al., 2006), postoperative Descemet's detachment occurred in 40-82% of patients on day one (Fukuda et al., 2011] and that stromal hydration persisted for up to 7 days.

AS-OCT has proved very useful in early recognition of localized or total graft dislocation in Descemet stripping automated endothelial keratoplasty (DSAEK), especially in eyes with corneal edema and limited anterior chamber visualization (Kymionis et al., 2010). The technique can also aid in diagnosis of eccentric trephination and inverse implantation of the donor (Ide et al., 2008; Kymionis et al., 2007; Suh et al., 2008). AS-OCT has been pivotal in documenting the cause of hyperopic shift in DSAEK eyes, which was induced by a high ratio of central graft thickness to peripheral graft thickness (Yoo et al., 2008). Epithelial in growth in refractive surgery can be confirmed by OCT images (Stahl et al., 2007).

OCT imaging and femtosecond laser-assisted surgeries are the most rapidly advancing technologies in modern day ophthalmology. Thickness is an important parameter in refractive surgery and no technique other than OCT can give accurate, uniform and predictable thickness measurements before, during and after surgery. The pachymetry map of AS-OCT can be used in femtosecond laser-assisted astigmatic keratotomy, LASIK enhancement and intrastromal tunnel preparation for intracorneal ring segments (Hoffart et al., 2009; Nubile et al., 2009). AS-OCT is very helpful in determining the accurate depth of the arcuate incisions, and in the postoperative follow up of patient with femtosecond astigmatic keratotomy and intracorneal ring segments. The images can explain the reasons behind unexpected postsurgical surprises (Yoo & Hurmeric., 2011). Femtosecond-assisted lamellar keratoplasty (FALK) is a highly promising refractive surgical technique that requires OCT data in accurate presurgical planning (Yoo et al., 2008). These procedures include anterior lamellar keratoplasty and deep anterior lamellar keratoplasty. AS-OCT imaging is the first step to measure the depth of anterior stromal scar and this determines the preparation of the donor and the recipient corneas. The morphology of the perfect match (donor and recipient) is confirmed by AS-OCT imaging. AS-OCT helps in careful planning of structure, thickness and shape of LASIK flap (Li et al., 2007; Rosas et al., 2011]. It is the depth of corneal incisions as obtained from AS-OCT that determines the success of new surgical techniques like femtosecond-assisted corneal biopsies, corneal tattooing and collagen crosslinking (Kymionis et al., 2009; Kanellopoulos et al.,2009; Nagy et al., 2009).

New platforms provide integrated OCT systems in the operating microscopes to perform the anterior segment procedures like corneal incisions, continuous curvilinear capsulorrhexis, nucleus softening, lens fragmentation, and focusing the laser in 3D manner in femtosecond-assisted cataract surgery (William et al., 2011; Wang et al., 2009).

Another milestone in OCT technology has been development of intraoperative 3D SD-OCT in the supine position (Dayani et al., 2009). This technique has been used for intraoperative evaluation of the presence of interface fluid between the donor and the recipient corneas in DSAEK.

3.1.2. Ocular surface disorders

OCT can be used for assessment of conjunctival and corneal tissue planes with high axial resolution. (Christopoulas et al., 2007 ; Shousha et al., 2011]. The technique acts as an adjuvant tool in diagnosing ocular surface squamous neoplasia and pterygia (Jeremy et al.,2012). OCT is in potential use for diagnosis and patient follow-up during the course of medical treatment and continued watch for recurrence of neoplasia without any need for repeated biopsies. Also the technique may be helpful in determining the extent of the tumor to facilitate its complete excision. AS-OCT guided subtenon injections of drugs like triamcinolone has reduced chances of inadvertent perforations and unwanted targets.

3.1.3. Glaucoma (anterior segment)

Recently Fourier-domain OCT has been used to examine the position, patency and the interior entrance site of the anterior chamber aqueous tube shunts. This high resolution OCT shows exact position of the AC entrance relative to Schwalbe's line and growth of fibrous tissue between the tube and the corneal endothelium. Such findings could not be seen with slit-lamp examination or lower resolution time-domain OCT. The tube position visualized by slitlamp examination differed from OCT finding (Jiang et al., 2012). OCT is also very helpful in correlating the clinical and visual field changes in glaucoma and ocular hypertension patients (Figure 7 & 8).

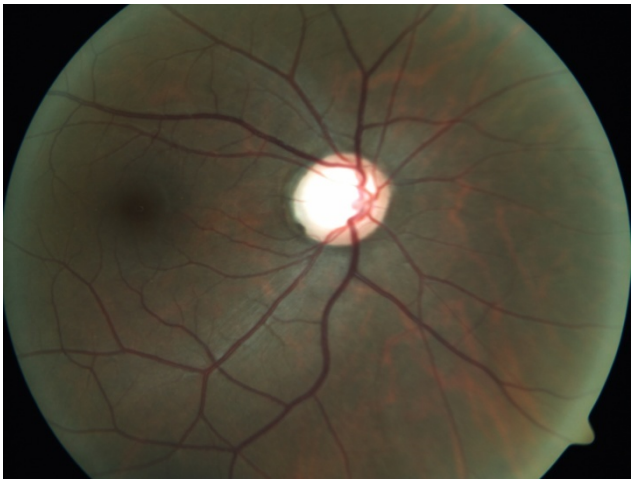

Figure 7. Fundus photo showing glaucomatous cupping temporaly.

http://dx.doi.org/10.5772/53961

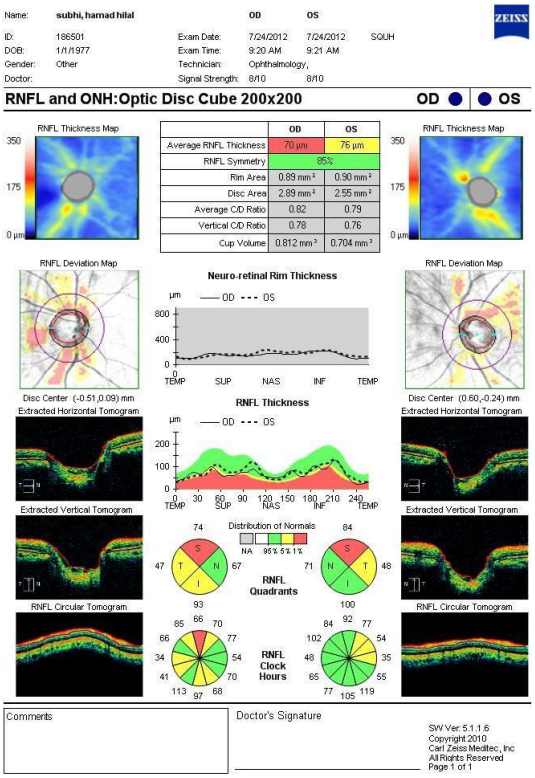

Figure 8. OCT printout of optic disc cube showing glaucomatous changes. The red measurements indicate abnormal thinning of RNFL, yellow areas represent borderline thickness of RNFL and green areas mean normal thickness of RNFL.

3.1.4. Ultrahigh Resolution (UHR) OCT

Ultrahigh resolution (UHR) OCT has been more practical and advantageous over confocal microscopy in making a clear distinction between morphologic and histopathologic features between normal and abnormal epithelium in ocular surface squamous neoplasia and pterygia. This is so because OCT is a noncontact method, has rapid image capture, and provides a cross-sectional view of the tissue. One of the recent clinical applications of UHR- OCT is the identification of the opaque bubble layer as a bright white area in mid stroma in femtosecond laser-assisted LASIK flap creation (Nordan et al., 2003). This technique has been of immense help to refractive surgeons in analyzing the flap integrity, indistinct flap interface or epithelial breakthrough in LASIK surgery (Seider et al., 2008; Ide et al., 2009; Ide et al., 2010). OCT is not a substitute for histopathologic specimens; however, it can be a potential noninvasive diagnostic adjuvant in diagnosis and surveillance of anterior segment pathologies of the eye.

3.2. Posterior segment

OCT now has a role in varied types of posterior segment pathologies (inflammatory, non-inflammatory, degenerative, vascular, traumatic, neoplastic, and metastatic) where the technique clearly defines the levels of various pathologic lesions in the posterior hyaloid, retina, retinal pigment epithelium and choroid, which in turn defines the mode and success of therapy. Such lesions may be superficial (epiretinal and vitreous membranes (Figures 6, 9 and 10), cotton wool spots, retinal hemorrhages, hard exudates (Figure 11), cysts (Figure 12), retinal fibrosis, and retinal scars (Figure 13) or deep (drusen-Figure 14), retinal pigment epithelial hyperplasia and detachment (Figure 15), intraretinal and subretinal neovascular membranes (Figure 16), scarring (figure 13) and pigmented lesions).

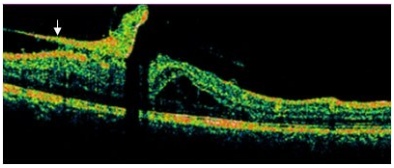

Figure 9. Epiretinal membrane (arrow) causing ripping of retinal tissue

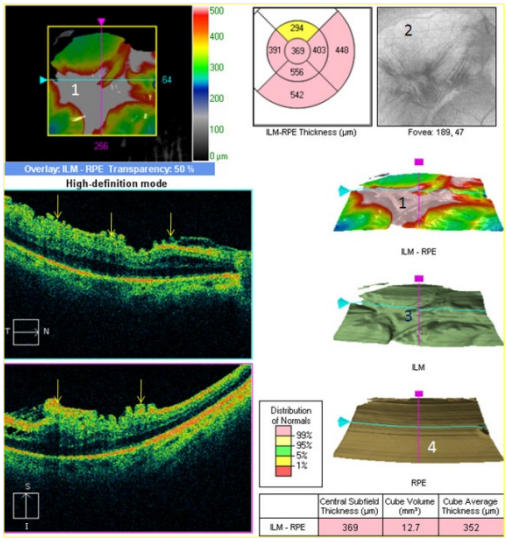

Figure 10. Retinal infoldings due to epiretinal membrane: 1: color map showing marked thickening (silver white and red areas) of ILM (internal limiting membrane)-RPE (retinal pigment epithelium) interface. 2: grey tone video image showing irregular surface with striations due to fibrous membrane. 3: ILM map showing marked irregularity due to contraction of the fibrous membrane. 4: A relatively intact RPE. Note the teeth-like infoldings of the retinal surface (yellow arrows) produced by ERM.

http://dx.doi.org/10.5772/53961

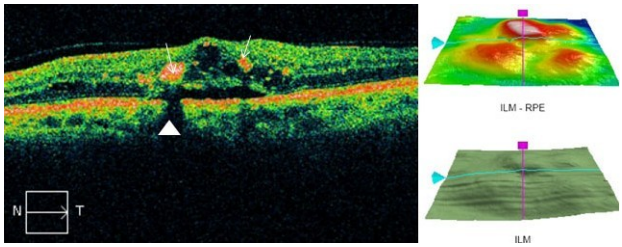

Figure 11. Hard exudates (white arrows). White triangle indicates the shadow cast by the exudate. The ILM-RPE color map shows three humps due to exudates.

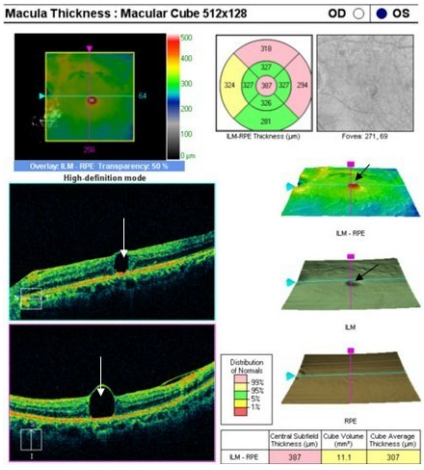

Figure 12. Solitary macular cyst (arrows). Note the blisters (black arrows) in the color map, corresponding to the cyst.

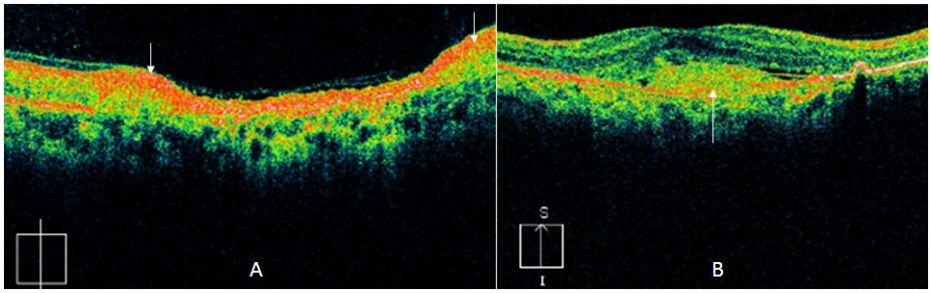

Figure 13. A: Extensive retinal scarring in a thin atrophic retina (orange red hyperreflective band between arrows). 13B- Scarring following involution of CNVM (arrow)

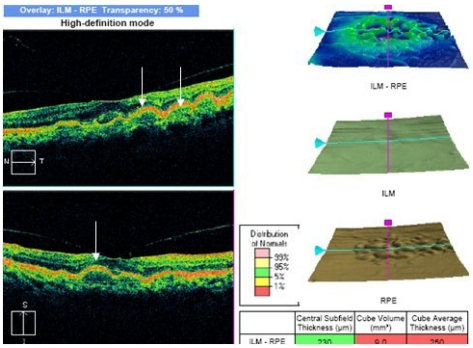

Figure 14. Drusen with bumps in the RPE (arrows). The drusen bumps produce characteristic humps in the color maps of ILM-RPE interface.

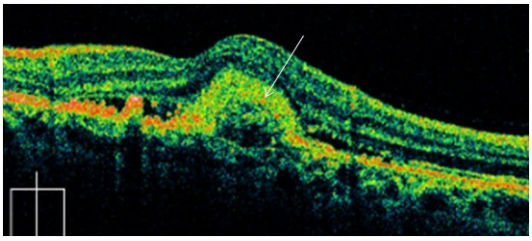

Figure 15. Thickened, irregular and detached RPE (arrow)

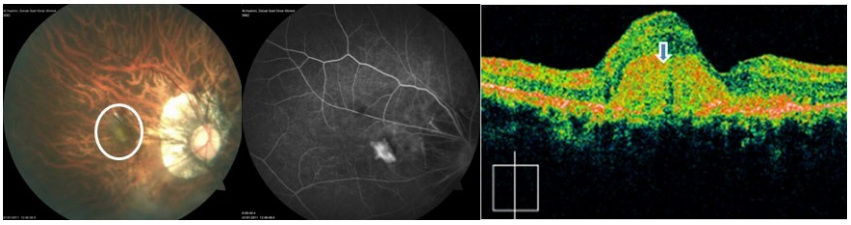

Figure 16. Myopic CNVM: Fundus photo gives a vivid description of myopic peripapillary atropy and a greyish white neovascular membrane in the macular area (encircled). FFA shows characteristic leakage corresponding to the area of neovascular membrane. OCT image depicts a hyperreflective subfoveal CNVM with increased retinal thickness (thick arrow).

3.2.1. Disorders of vitreous and posterior hyaloid

Vitreomacular traction (VMT) and vitreomacular adhesion (VMA) may be difficult to detect clinically. OCT is extremely helpful in such cases by showing hyperreflectivity. The traction by the membrane to the retina induces deformations of the retinal surface (Figure 17).

http://dx.doi.org/10.5772/53961

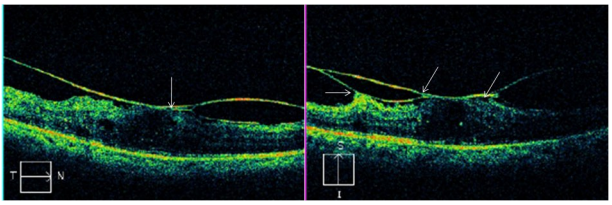

Figure 17. Vitreomacular traction. Note the multiple areas of traction caused by taught posterior hyaloid on retinal tissue (arrows).

3.2.2. Retinal edema

The most common primary cause of retinal thickening is edema. One of the major achievements of OCT has been quantitative assessment of retinal edema in terms of measuring its thickness and volume, evaluate the progression of the pathologic process, and monitor surgical or non-surgical intervention (Kang et al., 2004). Retinal edema may manifest in different categories:

Focal or diffuse edema: Common causes include diabetic retinopathy, central retinal venous occlusion, branch retinal venous occlusion, arterial occlusion, hypertensive retinopathy, preeclampsia, eclampsia, uveitis, retinitis pigmentosa and retraction of internal limiting membrane. OCT helps in diagnosis of edema in preclinical stage when there may be no or few visible changes.

Cystoid macular edema (CME): (Figure 18) Common causes of CME include diabetic retinopathy, age-related macular degeneration (ARMD), venous occlusions, pars planitis, Uveitis, pseudophakos, Irvine-Gass syndrome, Birdshot retinopathy and retinitis pigmentosa. OCT usually shows diffuse cystic spaces in the outer nuclear layer of central macula, and increased retinal thickness which is maximally concentric on the fovea (Mavrofrides et al., 2004).

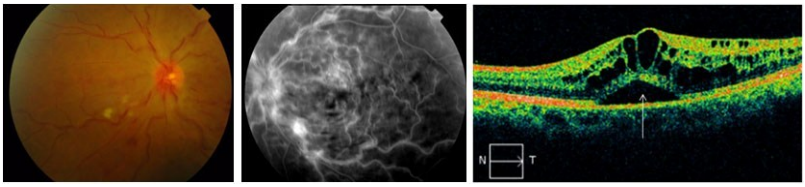

Figure 18. Cystoid macular edema in a patient with CRVO. Color fundus image shows disc hemorrhage, venous tortuosity, cotton wool exudates and retinal hemorrhages. FFA shows characteristic venous staining, leakge and blocked fluorescence due to underlying hemorrhage. OCT image depicts marked increase in retinal thickness due to edema. Note the intraretinal cysts and subretinal fluid (arrow).

Serous retinal detachment: The cysts of retinal edema over a period of time loose their walls and merge together forming single or multiple pools of fluid within retinal layers or between retinal pigment epithelium (RPE) and the sensory retina (Villate et al., 2004.) (Figure 19)

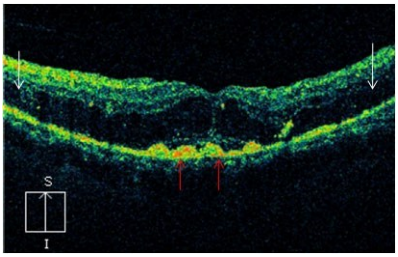

Figure 19. Serous retinal detachment (dark zone between white arrows) in a patient with severe nonproliferative diabetic retinopathy. Red arrows indicate subfoveal exudates.

3.2.3. Retinal pigment epithelial detachment (Figure 20)

Its pathophysiology involves passage of serous fluid from the choriocapillaries to the sub-RPE space or collection of blood under RPE causing its separation and elevation from the Bruch's membrane. OCT scans show a classical dome-shaped detachment of the RPE with intact contour in early stages (Figure 14).

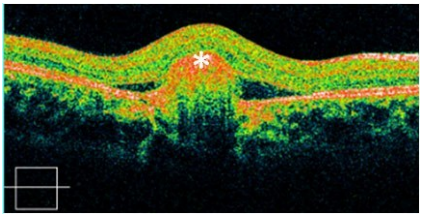

Figure 20. RPE detachment with hyperplasia (asterisk).

3.2.4. Epiretinal membranes (ERM)

Epiretinal membranes are fibroglial proliferations on the vitreo-retinal interface (Figure 10). They may be sequel of chronic intraocular inflammations, venous occlusions, trauma, post-surgical or may be idiopathic. OCT helps in confirming such membranes (Suzuki et al., 2003; Massin et al., 2000).

3.2.5. Secondary retinal lesions

OCT is important to document the presence, degree and extent of subretinal fluid (Villate et al., 2004), assessment of the level of retinal infiltrates and detect macular edema in patients with chronic uveitis where hazy media may prevent clinical examination to find the cause of reduced vision (Antcliff et al., 2002; Markomichelakis et al., 2004).

http://dx.doi.org/10.5772/53961

3.2.6. Retinoschisis

It is the separation or splitting of the neurosensory retina into an inner (vitreous) and outer (choroidal) layer with severing of neurons and complete loss of visual function in the affected area (Figure 21). Typically the split is in the outer plexiform layer. In reticular retinoschisis, which is less common, splitting occurs at the level of nerve fiber layer. Retinoschisis may be degenerative, myopic, juvenile or idiopathic. Presence of vitreoretinal traction is an important cause. OCT reveals wide space with vertical palisades and splitting of the retina into a thinner outer layer and thicker inner layer (Eriksson et al., 2004).

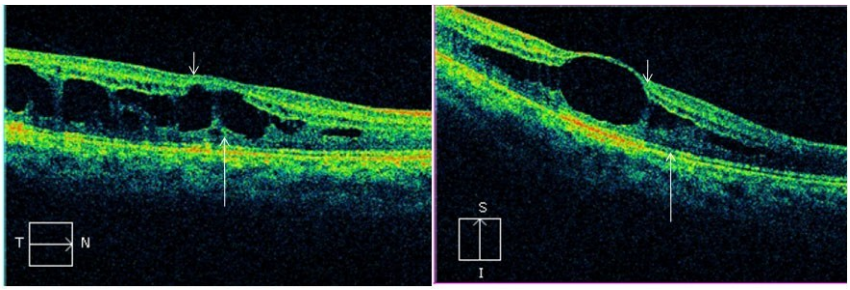

Figure 21. Retinoschisis: Note the splitting of retina into inner (small arrow) and outer layers (large arrow)

3.2.7. Macular holes

Lamellar hole: OCT depicts a homogenous increase in foveal and perifoveal retinal thickness, and presence of residual retinal tissue at the base of the hole (Figure 22).

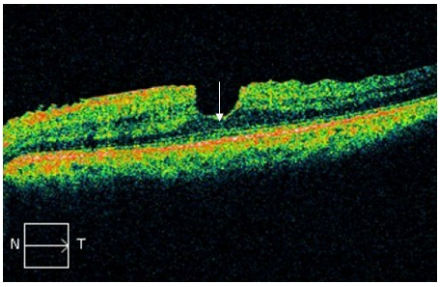

Figure 22. OCT image of a lamellar thickness macular hole with residual retinal tissue remaining between the base of the hole (arrow) and the RPE.

Full thickness macular hole: Majority of macular holes are idiopathic. Other causes include trauma, high myopia, vascular lesions (DR, venous occlusions, and hypertensive retinopathy) and subretinal neovascularization. OCT features in a full thickness macular hole include complete absence of foveal retinal reflectivity with no residual retinal tissue. Thickened retinal margins around the hole with reduced intraretinal reflectivity are clearly seen in such cases (Figure 23).

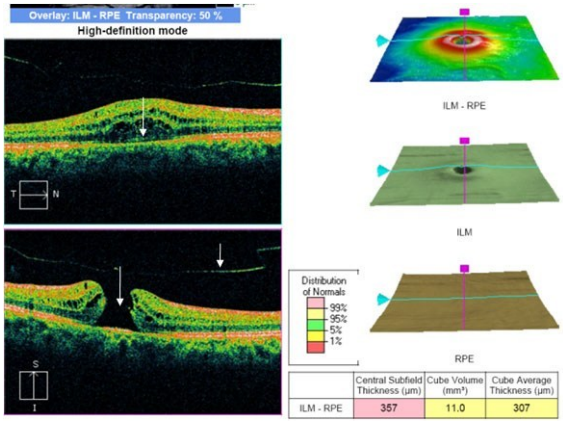

Figure 23. OCT (S-1): A full thickness macular hole (long arrow) in a diabetic patient with detached posterior hyaloid (short arrow). The T-N axis shows subretinal fluid collection (arrow). Color map: Top: red circle delineates edema; Middle: delineates a hole with elevated margins; Bottom: normal RPE.

3.2.8. Diabetic retinopathy

OCT is a vital tool in the hands of a vitreoretinal surgeon that aids in diagnosis, treatment and follow up of patients with DR. (Cruz-Villegas et al., 2004; Schaudig et al., 2000).

OCT features in DR include retinal edema, cotton wool spots, exudates, hemorrhages and ischemia. (Figures 24, 25)

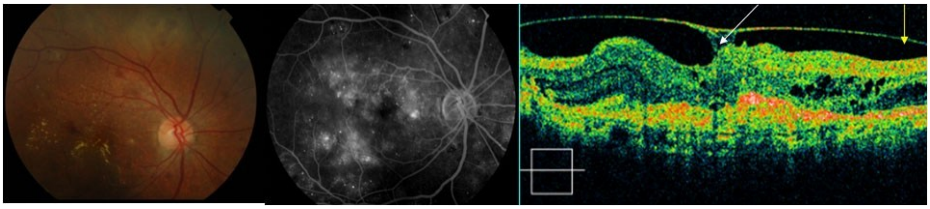

Figure 24. NPDR: color fundus photo shows classical moderate to severe NPDR with hemorrhages, exudates and maculopathy. FA shows retinal edema confined mainly to macular area. The foveal avascular zone is enlarged. OCT image shows VMA (white arrow), detached posterior hyaloid (yellow arrow), retinal thickening and intraretinal edema.

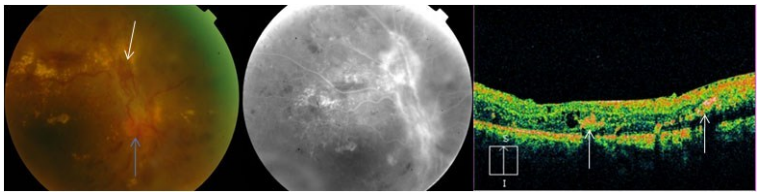

Figure 25. Proliferative diabetic retinopathy (PDR): Color fundus photo shows neovascularization of disc (NVD-blue arrow), neovascularization elsewhere (NVE- white arrow) and exudates. FFA shows corresponding leakge of dye. OCT image shows exudates (white arrows), a thin ERM and mild retinal edema.

3.2.9. Drug toxicities

OCT studies have started evaluating the retinal / macular toxic side effects of systemic drugs like hydroxychloroquine (Marmor., 2012), chloroquine (Korah and Kuriakose., 2008), tamoxifen (Hager et al., 2010), ethambutol (Menon et al., 2009), vigabatrin (Moseng et al., 2011) and tadalafil. (Coscas et al., 2012) Besides, the technique is being used in many research centers for studying retinal effects of a varied number of compounds in animal models.

3.2.10. Inflammatory lesions

OCT displays common associations of inflammation like edema, hemorrhage and scarring (Figure 26).

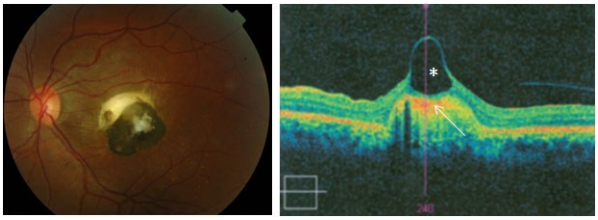

Figure 26. Color fundus image of a healed lesion of macular toxoplasmosis. OCT image shows scarring (arrow) associated with a retinal cyst (asterix).

3.2.11. Trauma and foreign bodies

Though clinical details of retinal foreign bodies may be quite discernible superficially, OCT gives a detailed description of the retinal layers affected and the sequel of impacted deeper

foreign bodies (Figure 27). The sequel of blunt eye injuries may be sub-clinical and OCT helps in determining the cause of unexplained reduced vision in such cases (Figure 27A).

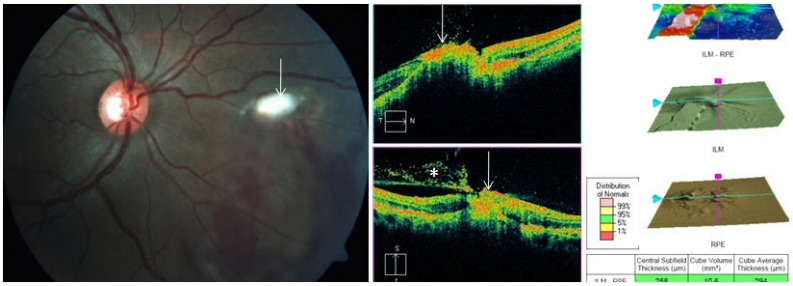

Figure 27. Embedded metallic retinal foreign body (arrow) with inferior retinal hemorrhage. OCT image showing retinal deformation with fibrosis (arrow) and vitreo-retinal debri (asterix). Note the deformation of the ILM-RPE color maps caused by fibrosis.

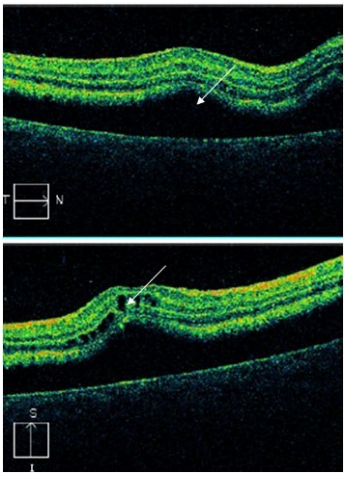

Figure 28. A(adobe): Submacular retinal detachment (arrows) in a 17 year old boy who sustained blunt eye injury after being hit by a football in the eye.

3.2.12. Neoplastic /metastatic lesions

OCT yields valuable information in such lesions especially when clinical examination may not be decisive due to media opacities (Figure 29).

http://dx.doi.org/10.5772/53961

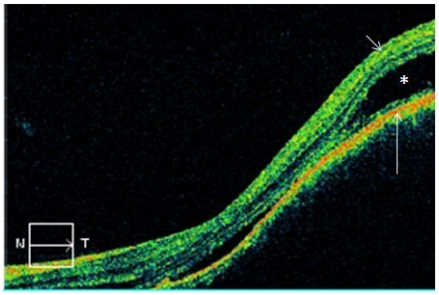

Figure 29. A 57 year old male with metastatic subretinal lesion. OCT image shows large dome shaped retinal (short arrow) and retinal pigment epithelium (long arrow) detachment associated with subretinal fluid (asterix).

The most exploited use of OCT has been in the field of treatment guidelines and response to therapies in diabetic retinopathy (figure 30), retinal vascular occlusions (figure 31), vascular lesions (figure 32), age related macular degeneration (figure 33), and intraocular inflammations. Physicians, who are used to OCT technology, feel more confident in diagnosing and managing such retinal disorders.

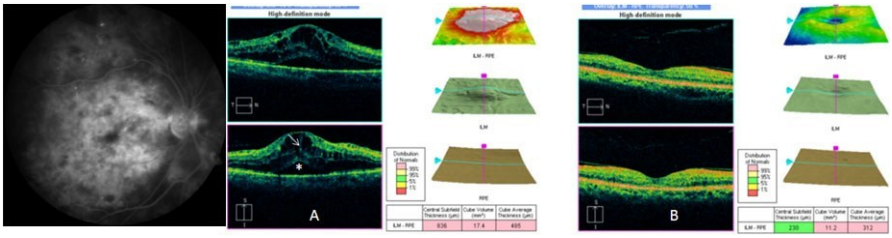

Figure 30. Diabetic macular edema: FFA shows diffuse leakage of dye in the macular area. OCT image (A): before treatment: diffuse macular edema with cystoid spaces (arrow) and subretinal fluid (asterix; central subfoveal thickness 836 microns). The septa (arrow) between retinal cysts are comprised of Müller's fibers. OCT image (B): dramatic improvement in retinal edema (central subfoveal thickness 230 microns) after intravitreal bevacizumab injections.

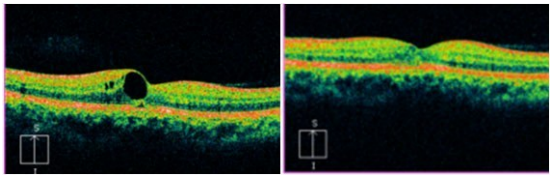

Figure 31. Left: Cystoid macular edema in a patient with branch retinal vein occlusion before therapy. Right: Two months after two intravitreal injections of bevacizumab the edema had resolved and normal foveal architecture was restored.

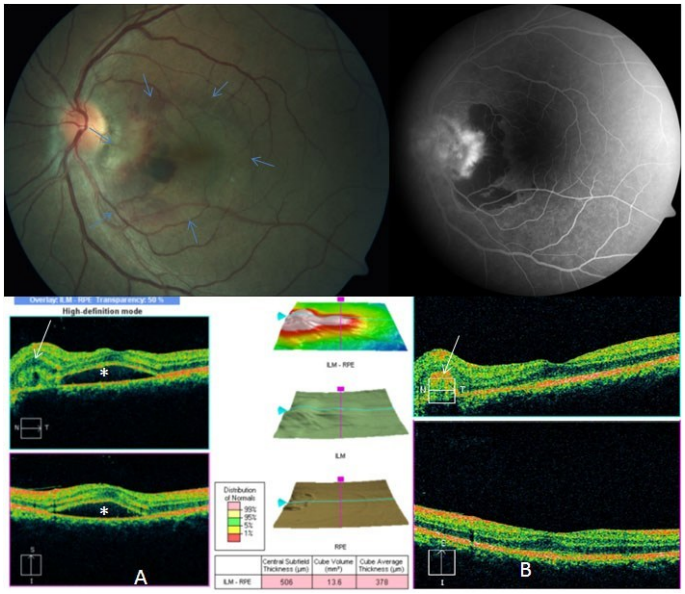

Figure 32. Juxtapapillary choroidal neovascular membrane in a 39 year old male. Color fundus photo shows the hemorrhage in deeper retinal layers with a circumscribed area of subretinal exudation (delineated by blue arrows). FFA shows leakge of dye from the juxtapapillary neovascular membrane. The dark area corresponds to blocked fluorescence due to hemorrhage. OCT image (A-before treatment) shows classical CNVM mound (arrow) with subretinal fluid in supero-temporal quadrant (asterix). OCT image (B) 18 weeks after three intravitreal injections of anti-VEGF drug ranibizumab shows brick-red organization (fibrosis) of CNVM (arrow) and resolution of subretinal fluid.

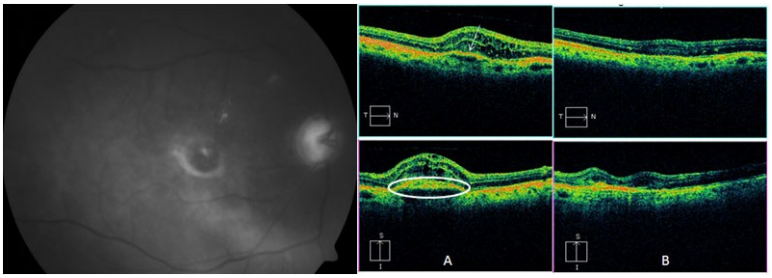

Figure 33. Age-related macular degeneration with CNVM. FFA shows a ring and central spot of hyperfluorescence in the macular area. OCT image A (30 April 2012) shows active CNVM (ovoid) with retinal edema and RPE deformity (arrow). The patient received two injections of intravitreal anti-VEGF drug ranibizumab. OCT image B (30 May 2012) shows marked regression of CNVM and retinal edema although retinal contour is altered.

Other therapeutic applications of OCT include accurate assessment of outcome of the effect of pharmacological or surgical interventions like photodynamic therapy (PDT), transpupillary thermotherapy, vitreoretinal surgery, anti-VEGF therapy, intravitreal steroid therapy and therapeutic Intravitreal implants (Rogers et al., 2002).

http://dx.doi.org/10.5772/53961

Recently OCT has confirmed benefit of intravitreal recombinant truncated human plasma serine protease ocriplasmin in treatment of non-symptomatic vitreomacular adhesion including macular hole (Decroos et al., 2012; Stalmans et al., 2010). OCT stays as sheet anchor in confirmation of successful surgical closure of macular holes (Jumper et al., 2000; Sato et al., 2003). In partial or unsuccessful surgeries, OCT evaluates the retinal anatomy to find reason for poor visual outcome.

4. Pediatric ophthalmology

SD-OCT allows detection of subclinical anatomic changes in neonates and infants, although experience on its use in retinopathy of prematurity (ROP) is limited (Chavala et al., 2009; Vinekar et al., 2010; Muni et al., 2010; Maldonado et al., 2010; Lee et al., 2011). Cystoid macular edema (CME) can be detected by SD-OCT in premature infants at risk for ROP but not when using indirect ophthalmoscopy (Maldonado et al., 2011). SD-OCT could be useful in detecting CME in neonates with mild and advanced ROP (Vinekar et al., 2011). Tomographic thickness measurements of cystoid macular edema in ROP predict the risk of requiring laser treatment or developing plus disease or ROP stage 3 (Maldonado et al., 2012). OCT is proving innovative in studying the macular characteristics in amblyopic eyes where the average thickness of foveolar neuroretina has been found to be larger than that of normal eyes (Wang et al., 2012)

5. Limitations of OCT

As with any new technology, limitations are inherent and so are with UHR-OCT. In anterior segment, leukoplakic or hyperreflective lesions often cast shadows on the underlying tissue. This may hide the diagnosis of underlying pathology.

6. Future strategies in OCT

Besides having OCT integrated slit lamp, increasing scanning speed and better axial resolution which would allow us to visualize tissues at the cellular level would be and should be the objective of future OCT imaging.

Author details

Nadia Al Kharousi, Upender K. Wali and Sitara Azeem

Department of Ophthalmology, College of Medicine and Health Sciences, Sultan Qaboos University, Muscat, Oman

References

[1] Huang D, Swanson EA, Lin CP, Schuman JS, Stinson WG, et al. (1991). Optical coherence tomography. Science, Vol. 254, No. 5035, (Nov), pp.1178-1181.

[2] Hrynchak P, Simpson T. (2007). Optical coherence tomography: an introduction to the technique and its use. Optom Vis Sci, Vol. 77, No. 7, (Jul), pp. 347-356.

[3] Ryan SJ. Retina, 4th edn, vol. 2. Elsevier Mosby 2006:1533-1556.

[4] Leung CK, Cheung CY, Weinreb RN, et al. (2009). Retinal nerve fiber layer imaging with spectral –domain optical coherence tomography: a variability and diagnostic performance study. Ophthalmology, Vol. 116, No. 7, (July), pp. 1257-63.

[5] Leung CK, Chiu V, Weinreb RN, et al. (2011). Evaluation of retinal nerve fiber layer progression in glaucoma: a comparison between spectral –domain and time – domain optical coherence tomography. Ophthalmology, Vol. 118, No.8, (Aug), pp. 1558 -62.

[6] Wang J, Conway TM, Yuan Y, Shen M, Cui L. (2010). Tear meniscus volume measured with ultra-high resolution OCT in dry eye after restasis treatment. ARVO Meeting Abstracts, 51 (Abstract 6266).

[7] Shen M, Wang MR, Yuan Y et al. (2010). SD-OCT with prolonged scan depth for imaging the anterior segment of the eye. Ophthal. Surg. Lasers Imaging, Vol. 41, No. 6, pp. S65–S69.

[8] Shousha MA, Perez VL, Wang J et al. (2010). Use of ultra-high-resolution optical coherence tomography to detect in vivo characteristics of Descemet's membrane in Fuchs' dystrophy. Ophthalmology, Vol. 117, No. 6, pp. 1220–1227.

[9] Goldsmith JA, Li Y, Chalita MR et al. (2005). Anterior chamber width measurement by high-speed optical coherence tomography Ophthalmology, Vol. 112, No. 2, pp. 238–244.

[10] Tang M, Chen A, Li Y, Huang D. (2010). Corneal power measurement with Fourier-domain optical coherence tomography. J. Cataract Refract. Surg., Vol. 36, No. 12, pp. 2115–2122.

[11] Alexandre SCR, Glen P. Sharpe, Hongli Yang, Marcelo TN, Claude FB, Balwantray CC. (2012). Optic Disc Margin Anatomy in Patients with Glaucoma and Normal Controls with Spectral Domain Optical Coherence Tomography. Ophthalmology Vol. 119, No.4, (Apr), pp. 738-747.

[12] Strouthidis NG, Yang H, Fortune B, et al. (2009). Detection of optic nerve head canal opening within histomorphometric and spectral domain optical coherence tomography data sets. Invest Ophthalmol Vis Sci, Vol. 50, No. 1, (Jan), pp. 214-23.

[13] Strouthidis NG, Yang H, Reynaud JF, et al. (2009). Comparison of clinical and spectral domain optical coherence tomography optic disc margin anatomy. Invest Ophthalmol Vis Sci, Vol. 50, No. 10, pp. 4709-18.

[14] Wali UK, Kharousi N. (2012). Selected Topics in Optical Coherence Tomography. In: Gangjun Liu, editor. Clinical Applications of Optical Coherence Tomography in Ophthalmology, Croatia; InTech publishing Inc; 2012, p 197-238.

[15] Shousha MA, Karp CL, Perez VL, et al. (2011). Diagnosis and management of conjunctival and corneal intraepithelial neoplasia using ultra high –resolution optical coherence tomography .Ophthalmology, Vol. 118,No. 8, pp. 1531 -7.

[16] Shousha MA, Perez VL, Wang J, et al. (2010). Use of ultra-high resolution Optical Coherence Tomography to detect in-vivo characteristics of Descemet's membrane in Fuch's dystrophy. Ophthalmology, Vol. 117, No.6, pp.1220-7.

[17] Cruz-Villegas V, Flynn HW Jr. (2004). Diabetic retinopathy. In: Schuman JS, Puliafito CA, Fujimoto JG, eds. Optical coherence tomography of ocular diseases. Thorofare, NJ: SLACK, Inc., 2004:157-214.

[18] Mavrofrides EC, Villate N, Rosenfeld PJ et al. [eds]. (2004). Optical coherence tomography of ocular diseases. In: Schuman JS, Puliafito CA, Fujimoto JG [eds]. Optical coherence tomography of ocular diseases. Thorofare, NJ: SLACK, Inc.; 2004:243-343.

[19] Mavrofrides EC, Cruz-Villegas V, Puliafito CA. (2004). Miscellaneous retinal diseases. In: Schuman JS, Puliafito CA, Fujimoto JG, eds. Optical coherence tomography of ocular diseases. Thorofare, NJ: SLACK, Inc.; 2004:457-482.

[20] Kang SW, Park CY, Ham DI. (2004). The correlation between fluorescein angiographic and optical coherence tomographic features in clinically significant diabetic macular edema. Am J Ophthalmol, Vol. 137, No. 2, (Feb), pp.313-322.

[21] Mavrofrides EC, Rogers AH, Truong S et al. (2005). Vitroretinal interface disorders. In: Schuman JS, Puliafito CA, Fujimoto JG, eds. Optical coherence tomography of ocular diseases. Thorofare, NJ: SLACK, Inc.; 2005: 57-102.

[22] Mori K, Gehlbach PL, Sano A, Deguchi T, Yoneya S. (2004). Comparison of epiretinal membranes of differing pathogenesis using optical coherence tomography. Retina, Vol. 24, No. 1, (Feb), pp. 57-62.

[23] Eriksson U, Larsson E, Holmstrom G. (2004). Optical coherence tomography in the diagnosis of juvenile X-linked retinoschisis. Acta Ophthalmol Scand, Vol. 82, No. 2, (Apr), pp. 218-23.

[24] Dawczynski J, Koenigsdoerffer E, Augsten R, Strobel J. (2007). Anterior optical coherence tomography: a non-contact technique for anterior chamber evaluation. Graefe's Arch Clin. Exp. Ophthalmol., Vol. 245, No. 3, pp. 423–425.

[25] Tan AN, Sauren LDC, de Brabander J et al. (2011). Reproducibility of anterior chamber angle measurements with anterior segment optical coherence tomography. Invest. Ophthalmol. Vis. Sci, Vol. 52, No. 5, pp. 2095–2099.

[26] Milla M, Piñero DP, Amparo F, Alió JL. (2011). Pachymetric measurements with a new Scheimpflug photography-based system: intraobserver repeatability and agreement with optical coherence tomography pachymetry. J. Cataract Refract. Surg, Vol. 37, No. 2, pp. 310–316.

[27] Nakagawa T, Maeda N, Higashiura R et al. (2011). Corneal topographic analysis in patients with keratoconus using 3-dimensional anterior segment optical coherence tomography. J. Cataract Refract. Surg, Vol. 37, No. 10, pp. 1871–1878.

[28] Baïkoff G, Lutun E, Wei J, Ferraz C. (2004). Anterior chamber optical coherence tomography study of human natural accommodation in a 19-year-old albino. J. Cataract Refract. Surg, Vol. 30, No. 3, pp. 696–701.

[29] Baïkoff G, Lutun E, Ferraz C, Wei J. (2004). Static and dynamic analysis of the anterior segment with optical coherence tomography. J. Cataract Refract. Surg, Vol. 30, No. 9, pp. 1843–1850.

[30] Dinc U, Gorgun E, Oncel B et al. (2010). Assessment of anterior chamber depth using visante optical coherence tomography, slitlamp optical coherence tomography, IOL master, pentacam and orbscan II. Ophthalmologica, Vol. 224, No. 6, pp. 341–346.

[31] Mamalis N. (2010). Phakic intraocular lenses. J. Cataract Refract. Surg, Vol. 36, No. 11, pp. 1805–1806.

[32] Lindland A, Heger H, Kugelberg M, Zetterström C. (2010). Vaulting of myopic and toric implantable collamer lenses during accommodation measured with Visante optical coherence tomography. Ophthalmology,Vol. 117, No. 6, pp. 1245–1250.

[33] Jagow von B, Kohnen T. (2009). Corneal architecture of femtosecond laser and microkeratome flaps imaged by anterior segment optical coherence tomography. J. Cataract Refract. Surg, Vol. 35, No. 1, pp. 35–41.

[34] Can I, Bayhan HA, Celik H, Bostancı CB. (2011). Anterior segment optical coherence tomography evaluation and comparison of main clear corneal incisions in microcoaxial and biaxial cataract surgery. J. Cataract Refract. Surg, Vol. 37, No. 3, pp. 490–500.

[35] Torres LF, Saez-Espinola F, Colina JM et al. (2006). In vivo architectural analysis of 3.2 mm clear corneal incisions for phacoemulsification using optical coherence tomography. J. Cataract Refract. Surg, Vol. 32, No. 37, pp. 1820–1826.

[36] Fukuda S, Kawana K, Yasuno Y, Oshika T. (2011). Wound architecture of clear corneal incision with or without stromal hydration observed with 3-dimensional optical coherence tomography. Am. J. Ophthalmol, Vol. 151, No. 3, pp. 413–419.

[37] Kymionis GD, Ide T, Donaldson K, Yoo SH. (2010). Diagnosis of donor graft partial dislocation behind the iris after DSAEK with anterior segment OCT. Ophthalmic

Surg. Lasers Imaging Vol. 9, pp. 1–2. Mar 9 :1-2 doi 10.3928/15428877.20100215-14[Epub ahead of print]

[38] Ide T, Yoo SH, Kymionis G, Shah P. (2008). Double Descemet's membranes after penetrating keratoplasty with anterior segment optical coherence tomography. Ophthalmic Surg. Lasers Imaging, Vol. 39, No. 5, pp. 422–425.

[39] Kymionis GD, Suh LH, Dubovy SR, Yoo SH. (2007). Diagnosis of residual Descemet's membrane after Descemet's stripping endothelial keratoplasty with anterior segment optical coherence tomography. J. Cataract Refract. Surg, Vol. 33, No. 7, pp. 1322–1324.

[40] Suh LH, Yoo SH, Deobhakta A et al. (2008). Complications of Descemet's stripping with automated endothelial keratoplasty: survey of 118 eyes at One Institute. Ophthalmology, Vol. 115, No. 9, pp. 1517–1524.

[41] Yoo SH, Kymionis GD, Deobhakta AA et al. (2008). One-year results and anterior segment optical coherence tomography findings of Descemet stripping automated endothelial keratoplasty combined with phacoemulsification. Arch Ophthalmol, Vol. 126, No. 8, pp. 1052–1055.

[42] Stahl JE, Durrie DS, Schwendeman FJ, Boghossian AJ. (2007). Anterior segment OCT analysis of thin IntraLase femtosecond flaps. J. Refract. Surg, Vol. 23, No. 6, pp. 555–558.

[43] Hoffart L, Proust H, Matonti F, Conrath J, Ridings B. (2009). Correction of postkeratoplasty astigmatism by femtosecond laser compared with mechanized astigmatic keratotomy. Am. J. Ophthalmol, Vol. 147, No. 5, pp. 779–787.

[44] Nubile M, Carpineto P, Lanzini M et al. (2009). Femtosecond laser arcuate keratotomy for the correction of high astigmatism after keratoplasty. Ophthalmology, Vol. 116, No. 6, pp. 1083–1092.

[45] Yoo SH, Hurmeric V. (2011). Femtosecond laser-assisted keratoplasty. Am J Ophthalmol, Vol. 151, No. 2, pp. 190–191.

[46] Yoo S, Kymionis GD, Koreishi A et al. (2008). Femtosecond laser-assisted sutureless anterior lamellar keratoplasty. Ophthalmology Vol. 115, No. 8, pp. 1303–1307.

[47] Li Y, Netto M, Shekhar R, Krueger R, Huang D. (2007). A longitudinal study of LASIK flap and stromal thickness with high-speed optical coherence tomography. Ophthalmology Vol. 114, No. 6, pp. 1124–1132.

[48] Rosas SCH, Li Y, Zhang X et al. (2011). Repeatability of laser in situ keratomileusis flap thickness measurement by Fourier-domain optical coherence tomography. J. Cataract Refract. Surg, Vol. 37, No. 4, pp. 649–654.

[49] Kymionis GD, Ide T, Galor A, Yoo SH. (2009). Femtosecond-assisted anterior lamellar corneal staining-tattooing in a blind eye with leukocoria. Cornea, Vol. 28, No. 2, pp. 211–213.

[50] Kanellopoulos AJ. (2009). Collagen cross-linking in early keratoconus with riboflavin in a femtosecond laser-created pocket: initial clinical results. J. Refract. Surg, Vol. 25, No. 11, pp. 1034–1037.

[51] Nagy Z, Takacs A, Filkorn T, Sarayba M. (2009). Initial clinical evaluation of an intraocular femtosecond laser in cataract surgery. J. Refract. Surg, Vol. 25, No. 12, pp. 1053–1060.

[52] William WC, Juan FB, Rafael F et al. (2011). Facilitation of nuclear cataract removal by femtosecond laser pretreatment. ASCRS, (Abstract 982342).

[53] Wang J, Jiao S, Ruggeri M, Shousha MA, Chen Q. (2009). In situ visualization of tears on contact lens using ultra high resolution optical coherence tomography. Eye Contact Lens, Vol. 35, No. 2, pp. 44–49.

[54] Dayani PN, Maldonado R, Farsiu S, Toth CA. (2009). Intraoperative use of handheld spectral domain optical coherence tomography imaging in macular surgery. Retina, Vol. 29, No. 10, pp. 1457–1468.

[55] Christopoulos V, Kagemann L, Wollstein G, et al. (2007). In vivo corneal high–speed, ultra high resolution optical coherence tomography. Arch Ophthalmol, Vol. 125, No . 8, pp. 1027-35.

[56] Jeremy ZK, Carol LK, Shousha MA, Galor A, Rodrigo AH, Dubovy SR et al. (2012). Ultra–High Resolution optical coherence tomography for differentiation of ocular surface squamous neoplasia and pterygia. Ophthalmology, Vol. 119: No. 3, (Mar), pp. 481-486.

[57] Jiang C, Li Yan, Huang D, Brian AF. (2012). Study of Anterior Chamber Aqueous tube shunt by Fourier–Domain Optical coherence tomography. Journal of Ophthalmology, doi:10.1155/2012/189580

[58] Nordan LT, Slade SG, Baker RN, Suarez C, Juhasz T, Kurtz R. (2003). Femtosecond laser flap creation for laser in situ keratomileusis: six-month follow-up of initial U.S. clinical series. J. Refract. Surg, Vol. 19, No. 1, pp. 8–14.

[59] Seider M, Ide T, Kymionis GD, Culbertson WW, O'Brien T, Yoo S. (2008). Epithelial breakthrough during IntraLase flap creation for laser in situ keratomileusis. J. Cataract Refract. Surg, Vol. 34, No. 5, pp. 859–863.

[60] Ide T, Yoo SH, Kymionis GD, Haft P, O'Brien TP. (2009). Second femtosecond laser pass for incomplete laser in situ keratomileusis flaps caused by suction loss. J. Cataract Refract. Surg, Vol. 35, No. 1, pp. 153–157.

[61] Ide T, Wang J, Tao A et al. (2010). Intraoperative use of three-dimensional spectral-domain optical coherence tomography. Ophthalmic Surg. Lasers Imaging, Vol. 41, No. 2, pp. 250–254.

[62] Villate N, Mavrofrides EC, Davis J. (2004). Chorioretinal inflammatory diseases. In: Schuman JS, Puliafito CA, Fujimoto JG, eds. Optical coherence tomography of ocular diseases. Thorofare, NJ: SLACK, Inc.; 2004:371-412.

[63] Suzuki T, Terasaki H, Niwa T. (2003). Optical coherence tomography and focal macular electroretinogram in eyes with epiretinal membrane and macular pseudohole. Am J Ophthalmol, Vol. 136, No. 1, (Jul), pp. 62-67

[64] Massin P, Allouch C, Haouchine B, Metge F, Pâques M, et al. (2000). Optical coherence tomography of idiopathic macular epiretinal membranes before and after surgery. Am J Ophthalmol, Vol. 130, No. 6, (Dec), pp. 732-739.

[65] Antcliff RJ, Stanford MR, Chauhan DS, Graham EM, Spalton DJ, et al. (2002). Comparison between Optical coherence tomography and fundus fluorescein angiography for the detection of cystoid macular edema in patients with uveitis. Ophthalmology, Vol. 107, No. 3, (Mar), pp. 593-599.

[66] Markomichelakis NN, Halkiadakis I, Pantelia E, Peponis V, Patelis A, et al. (2004). Patterns of macular edema in patients with uveitis: qualitative and quantitative assessment using Optical coherence tomography. Ophthalmology, Vol. 111, No. 5, (May), pp. 946-953.

[67] Schaudig UH, Glaefke C, Scholz F, Richard G. (2000). Optical coherence tomography for retinal thickness measurement in diabetic patients without clinically significant macular edema. Ophthalm Surg Lasers, Vol. 31, No. 3, (May-Jun) pp. 182-186.

[68] Marmor MF. (2012). Comparison of screening procedures in hydroxychloroquine toxicity. Arch Ophthalmol, Vol. 130, No. 4, pp. 461-9

[69] Korah S, Kuriakose T. (2008). Optical coherence tomography in a patient with chloroquine-induced maculopathy. Indian J Ophthalmol, Vol. 56, No. 6, (Nov-Dec), pp. 511-3

[70] Hager T, Hoffmann S, Seitz B. (2010). Unusual symptoms for tamoxifen –associated maculopathy. Ophthalmologe, Vol. 107, No. 8, pp. 750-2.

[71] Menon V, Jain D, Saxena R, Sood R. (2009). Prospective evaluation of visual function for early detection of ethambutol toxicity. Br J Ophthalmol, Vol. 93, No. 9, pp. 1251-4

[72] Moseng L, Saeter M, Mørch-Johnsen GH, Hoff JM, Gajda A, Brodtkorb E, et al. (2011). Retinal nerve fibre layer attenuation: clinical indicator for vigabatrin toxicity. Acta Ophthalmol, Vol. 89, No. 5, pp. 452-8.

[73] Coscas F, Coscas G, Zucchiatti I, Bandello F, Soubrane G, Souied E. (2012). Optical coherence tomography in tadalafil-associated retinal toxicity. Eur J Ophthalmol, Feb7:0.doi:10.5301/ejo.5000127.

[74] Rogers AH, Martidis A, Greenberg PB, Puliafito CA. (2002). Optical coherence tomography findings following photodynamic therapy of choroidal neovascularisation. Am J Ophthalmol, Vol. 134, No. 4, (Oct), pp. 566-576.

[75] Decroos FC, Toth CA, Folgar FA, Pakola S, Stinnett SS, Heydary CS, et al. (2012). Characterization of vitreoretinal interface disorders using OCT in the interventional phase 3 trials of ocriplasmin. Invest Ophthalmol Vis Sci. (Aug 9). [Epub ahead of print]

[76] Stalmans P, Delaey C, de Smet MD, van Dijkman E, Pakola S. (2010). Intravitreal injection of microplasmin for treatment of vitreomacular adhesion: results of a prospective, randomized, sham-controlled phase II trial (the MIVI-IIT trial). Retina, Vol. 30, No. 7, pp. 1122-7.

[77] Jumper JM, Gallemore RP, McCuen BW 2nd, Toth CA. (2000). Features of macular hole closure in the early postoperative period using optical coherence tomography. Retina, Vol. 20, No. 3, pp. 232-237.

[78] Sato H, Kawasaki R, Yamashita H. (2003). Observation of idiopathic full-thickness macular hole closure in early postoperative period as evaluated by optical coherence tomography. Am J Ophthalmol, Vol. 136, No. 1, (Jul), pp. 185-187.

[79] Chavala SH, Farsiu S, Maldonado R ,Wallace DK, Freedman SF ,Toth CA. (2009). Insights into advanced retinopathy of prematurity using handheld spectral domain optical coherence tomography. Ophthalmology Vol. 116, No. 12, pp. 2448 -2456

[80] Vinekar A, Sivakumar M, Shetty R, et al. (2010). A novel technique using spectral domain optical coherence tomography (Spectralis, SD-OCT+HRA) to image supine non –anaesthetized infants: utility demonstrated in aggressive posterior retinopathy of prematurity. Eye, Vol. 24, No. 2, pp. 379-382

[81] Muni RH, Kohly RP, Charonis AC, Lee TC. (2010). Retinoschisis detected with handheld spectral domain optical coherence tomography in neonates with advanced retinopathy of prematurity. Arch Ophthalmol, Vol. 128, No. 1, pp. 57-62

[82] Maldonado RS, Izatt JA, Sarin N, et al. (2010). Optimizing handheld spectral domain optical coherence tomography imaging for neonates and infants and children. Invest. Ophthalmol. Vis. Sci. Vol. 51, No. 5, pp. 2678 -2685.

[83] Lee AC, Maldonado RS , Sarin N, et al. (2011). Macular features from spectral domain optical coherence tomography as an adjunct to indirect ophthalmoscopy in retinopathy of prematurity. Retina, Vol. 31, No.8, pp. 1470 -1482

[84] Maldonado RS, O' Connell RV, Sarin N, et al. (2011). Dynamics of human foveal development after premature birth. Ophthalmology, Vol. 118, No.12, (Dec), pp. 2315-25.

[85] Vinekar A, Avadhani K, Sivakumar M et al. (2011). Understanding clinically undetected macular changes in early retinopathy of prematurity on spectral domain optical coherence tomography. Invest. Ophthalmol. Vis. Sci. Vol. 52, No.8, (Aug), pp. 5183-5188

[86] Maldonado RS, O' Connell R, Ascher SB, Sarin N, Freedman SF, et al. (2012). Spectral –domain optical coherence tomographic assessment of severity of cystoid macular

edema in retinopathy of prematurity. Arch Ophthalmol, Vol.130, No. 5, (May), pp. 569 -78

[87] Wang XM, Cui DM, Yang X, Huo LJ, Liu X, et al.(2012). Characteristics of the macula in amblyopic eyes by optical coherence tomography. Int J Ophthalmol, Vol. 5, No. 2, pp.172-176.